Improved Fault Detection and Isolation of Small Faults using Multiple Residual Generators and Complex Detection Hypotheses: Case Study of an Electro-Hydraulic Aerospace Actuator

Desham Mitra[1], Pulak Halder[2], and Siddhartha Mukhopadhyay[3]

[1,3]*Department of Electrical Engineering, IIT Kharagpur, India*
ddesham@iitkgp.ac.in
smukh@ee.iitkgp.ac.in

[2]*RCI, DRDO, India*
pulak.halder@rcilab.in

ABSTRACT

Failure prevention in safety and mission critical applications is enabled by Fault Detection and Isolation (FDI) systems. The performance of FDI is characterized by the associated Probability of Detection (P_D) and Probability of False Alarm (P_{FA}). This paper presents a study on the performance of FDI systems through Receiver Operating Characteristic (ROC) plots. It is shown that fault decisions made by testing complex detection hypotheses involving residual signals generated by multiple state and parameter estimators can enhance the performance of the FDI system. The study illustrates the various factors involved in the design of this system in terms of the choice of residual generators, detection hypotheses as well as their decision thresholds and the detection speed. The numerical implementation of the FDI system is made and tested for a detailed nonlinear simulation of a real Electro-Hydraulic Actuator (EHA) for aerospace applications.

1. INTRODUCTION

For many safety and mission critical systems detecting faults at an early stage to avoid failures is of great importance. This involves early detection and isolation of weak fault signatures in presence of noise and unmodelled dynamics. This is difficult and can lead to false alarms (Type I error) and missed detection (Type II error). Over the past several decades various methods of fault detection and isolation have been reported. An early survey on fault diagnosis is done by Frank (1990). Blanke (2006), Isermann (2006) and Ding (2008) capture the developments of the theory of fault detection and diagnosis using dynamic models over the next two decades. These methods have also been applied in the context of aerospace Electro-Hydraulic Actuators (An & Sepehri, 2003, 2005, Chinniah et. al., 2003 and Chinniah, 2004). However, most of these works reported in the literature suffer from the following shortcomings:

1. These present an algorithm for detection of a single fault. In reality there is always a possibility of occurrence of faults of various types. A fault detector designed to detect a particular fault (say fault A) is likely to indicate presence of fault A due to noise in absence of faults or due to occurrence of a different fault. This effect is enhanced when the detection thresholds are kept low to enable detection of small faults. These scenarios are not addressed.

2. It is well known that improvements in performance hypothesis testing can be achieved by involving multiple residuals corrupted by weakly correlated noise sequences. To leverage these various appropriate issues in the design of such FDI systems need to be studied. Such studies are conspicuous by absence.

ROC plots (Kay, 1998) capture the P_D-P_{FA} performance of detectors. ROC based characterization of performance have been reported in the medical field (Metz, 2006, Kumar & Indrayan, 2011, Hajian-Tilaki, 2013). In the context of engineering systems, recently Trachi et. al., (2017) have applied ROC techniques for designing a detector to detect bearing faults and broken rotor bar faults for induction machine. No attempt, however, has been made towards isolation of a fault that can occur from among set of multiple possible faults.

In this paper design of an FDI system for an EHA used in aerospace applications is considered. EHAs (Merritt, 1967) are widely used in safety and mission critical applications in

the aerospace industry. Five typical faults for the EHA (three sensor bias faults and two parametric faults) have been considered out of which three faults have been successfully isolated using three typical measurements available in the actuator with known nominal values of parameters. The main contributions of this paper are as follows:

1. It demonstrates the possibility of formulating multiple estimators for residual generation with multiple sensor measurements and a dynamic model of the system. Three different Dual EKF based estimators have been formulated utilizing various subsets of measurements to generate ten residuals. It is assumed that any single fault out of the five can occur at a time. This is a reasonable assumption since the faults are independent and detection times are negligible compared to the time intervals over which faults develop.

2. Complex detection hypotheses are designed using several residuals generated from these three estimators to isolate the faults. Systematic method of developing these hypotheses based on the so called D-Matrix (Isermann, 2006), which captures the sensitivity of each residual to various faults, is illustrated.

3. Finally the decision thresholds are chosen based on the corresponding P_D-P_{FA} performances as seen from ROC plots.

2. MODELLING OF AN ELECTRO-HYDRAULIC ACTUATOR

Figure 1 shows a nonlinear dynamic model of an EHA used in thrust vector control of a rocket. A linearized version of this model is available in Halder (2012). To model the second order servo valve dynamics two states d_a and d_b are introduced where d_a denotes valve stroke. The equations describing the system are:

$$
\begin{aligned}
\dot{x} &= v + w_1 \\
\dot{v} &= -\frac{981\times 5730\ K_{SD}}{m {l_T}^2}\, x - \frac{981\, b_{eq}}{m}\, v + \frac{981\, a}{m}\, P_m + w_2 \\
\dot{P}_m &= -\frac{4\beta a}{V_o}\, v - \frac{4\beta C_{2g}}{V_o}\, P_m + \frac{4\beta}{V_o} Q_d + w_3 \\
Q_d &= d_a Co \left\{P_s - P_m \operatorname{sgn}(d_a)\right\}^{1/2} \\
\dot{d}_a &= d_b + w_4 \\
\dot{d}_b &= -\omega_v^2 d_a - 1.4\,\omega_v d_b + r\omega_v^2 K_v ks\, x_n + r\omega_v^2 ks K_v K_p K_{pfb}\, x_c + w_5 \\
\dot{x}_n &= -K_i K_{pfb}\, x - K_p K_{pfb}\, v + K_i K_{pfb}\, x_c + w_6
\end{aligned}
\qquad (1)
$$

where $w_i, (i = 1,2,\ldots,6)$ represent unmodelled dynamics and input disturbances of a well characterized EHA.

Also one can write:

$$
\begin{aligned}
\dot{d}_b &= -\omega_v^2 d_a - 1.4\,\omega_v d_b + r\, ks\, \omega_v^2\, i_c \\
i_c &= (x_c - x) K_{pfb} + \left(K_p + \frac{K_i}{s}\right) K_v \\
&= K_{pfb}\left(-K_p x + \frac{K_i}{s}(x_c - x)\right) K_v + K_v K_p K_{pfb}\, x_c
\end{aligned}
\qquad (2)
$$

In (Eq. 1) x_n is an artificial state variable described in terms of x expressed as $K_{pfb}\left(-K_p x + \frac{K_i}{s}(x_c - x)\right)$. The signals Q_d and i_c are limited within maximum and minimum values to incorporate saturation. Overlap condition of the valve spool is modelled using a dead zone. All continuous system equations are discretized with a sampling time of 10 microseconds since the bandwidth of the innermost pressure loop turns out to be very high. This complete system is modelled in numerically MATLAB Simulink.

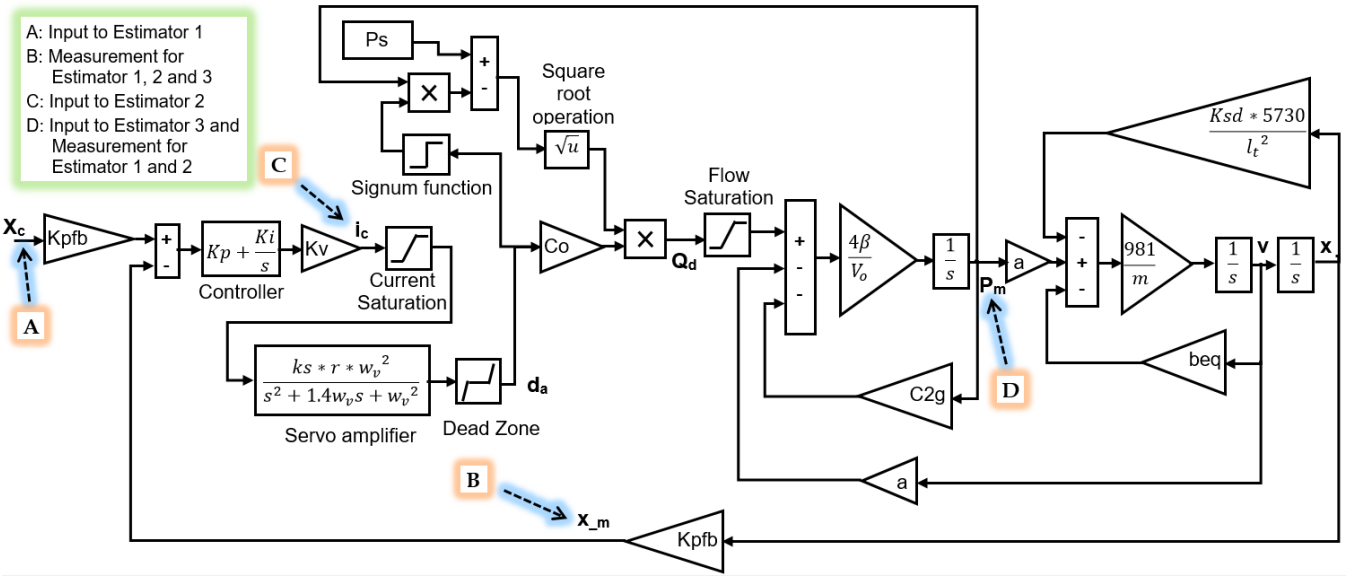

Figure 1. Signal Flow Diagram of an Electro-Hydraulic Actuator

The input to the EHA is the reference actuator position x_c obtained from the autopilot which is in turn driven by the guidance loop. The input x_c chosen for this system is derived from a white noise sequence with mean 2 and variance 0.5 sampled at 0.1 seconds, passed through a low pass filter with 3dB cut-off frequency of 0.5 Hz.

3. DESIGN OF MULTIPLE RESIDUAL GENERATORS

In this paper a dual estimator (Wan & Nelson, 2001) is used. It generates two types of residuals; namely, measurement residuals, being the difference between measured variables and their estimates, and the parameter residuals, being the difference between nominal values and estimated values of parameters. These residuals, computed online, are used in various complex detection hypotheses to isolate multiple faults. Figure 2 shows the bootstrapped structural representation of a dual EKF which has been used here to generate residuals.

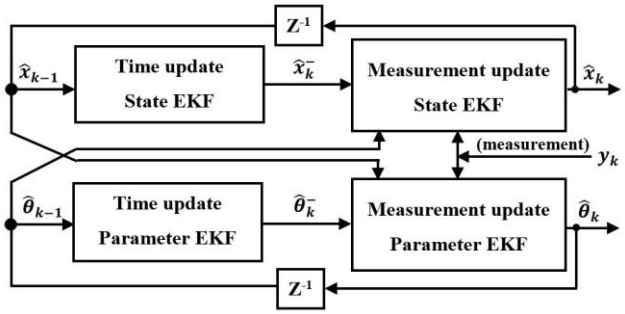

Figure 2. Structure of the Dual EKF estimator

Let $\{Kj, Rxj \mid j = 1,2,3\}$ and $\{Bj, Rpj \mid j = 1,2\}$ denote residuals of K_{SD}, x, β and P_m for the j^{th} residual generator, respectively. v_1, v_2 and v_3 represent measurement noises in the sensors. All measured values of variables are denoted as <variable>_m. The various residual generating estimators are described below. The inputs and measurements of the various estimators have also been indicated in Figure 1 for clarity.

Estimator 1

Input: Reference actuator position: x_c

Measurements:

Actuator position sensed by LVDT: $x_{\_m} = K_{pfb}\, x + v_1$

Differential pressure: $P_{m\_m} = P_m + v_2$

States: x, v, P_m, d_a, d_b and x_n

Model equations: Same as Eq. (1)

Residuals: *Rx1, Rp1* and *K1* and *B1*

Estimator 2

Input: Driving current of servo valve: $i_{c\_m} = i_c + v_3$

Measurements: Same as Estimator 1

States: x, v, P_m, d_a and d_b

Model equations:

$$\dot{x} = v + w_1$$

$$\dot{v} = -\frac{981 \times 5730\ K_{SD}}{m l_T{}^2}\, x - \frac{981\, b_{eq}}{m}\, v + \frac{981\, a}{m}\, P_m + w_2$$

$$\dot{P}_m = -\frac{4\beta a}{V_o}\, v - \frac{4\beta C_{2g}}{V_o}\, P_m + \frac{4\beta d_a Co}{V_o}\left\{P_s - P_m \operatorname{sgn}(d_a)\right\}^{1/2} + w_3$$

$$\dot{d}_a = d_b + w_4$$

$$\dot{d}_b = -\omega_v^2 d_a - 1.4\,\omega_v d_b + \omega_v^2\, i_{c\_m}$$

Residuals: *Rx2, Rp2* and *K2, B2*

Estimator 3

Input: Differential pressure: $P_{m\_m} = P_m + v_2$

Measurement: $x_{\_m} = K_{pfb}\, x + v_1$

States: x and v

Model equations:

$$\dot{x} = v + w_1$$

$$\dot{v} = -\frac{981 \times 5730\ K_{SD}}{m l_T{}^2}\, x - \frac{981\, b_{eq}}{m}\, v + \frac{981\, a}{m}\, P_{m\_m} + w_2$$

Residuals: *Rx3* and *K3*

3.1. Faults

A total of five faults are chosen whose characteristics are shown in Table 1. F1, F2 and F3 are constant sensor bias faults in the LVDT, Pressure and Current sensor outputs, respectively. F4 and F5 are parametric faults due to increase in seal stiffness and decrease in fluid bulk modulus faults, respectively. Here FC stands for Fault Code. Units of fault magnitudes are same as their corresponding faulty variables. NA means Not Applicable.

Table 1. List of Faults Considered

FC	Faulty Variable	Measurement Range/ Nominal Parameter	Sensor Noise (μ,σ)	Fault Magnitude Range (Step)
F1	$x_{\_m}$	0 – 5 V	(0, 0.05)	0 to +0.11 (0.03)
F2	P_{m_m}	0 – 208 ksc	(0, 2)	0 to +5.0 (1.0)
F3	i_{c_m}	0 – 10 mA	(0, 0.032)	0 to +1.0 (0.2)
F4	K_{SD}	800 kgm/deg	NA	0 to +100 (20)
F5	β	7000 kg/sq.cm	NA	0 to -2000 (-400)

For preventing estimator transients to get reflected on the residuals and yet to keep simulation intervals within reasonable limits, ramp type faults are introduced at a specific time instant (at t = 6 seconds). The magnitudes of the faults linearly develop from 6 to 8 seconds and become steady after 8 seconds. Figures 3 and 4 show the behavior of residuals when subjected to a fault F1 of magnitude +0.09V and a fault F5 of magnitude -1200 kg/sq.cm, respectively.

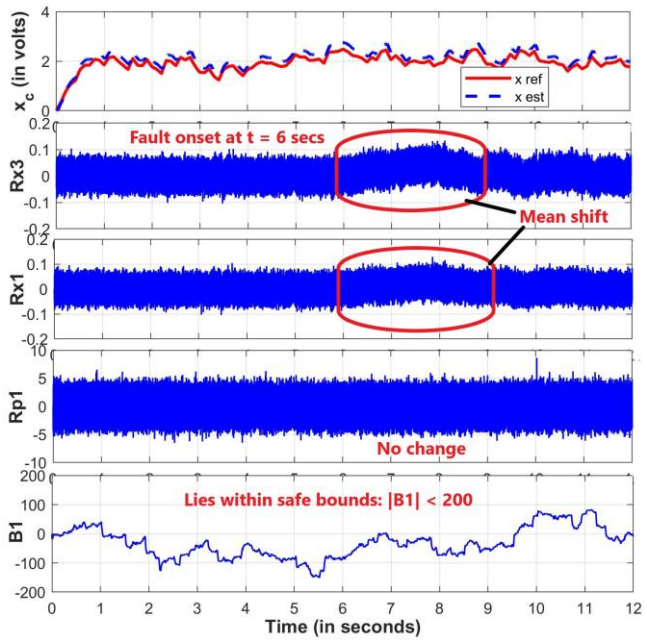

Figure 3. Effect of F1 = +0.09V on residuals

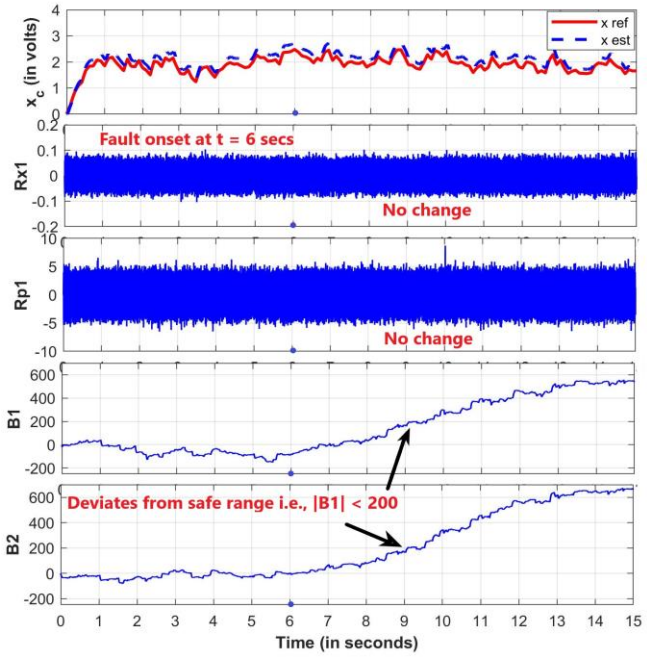

Figure 4. Effect of F5 = -1200 kg/sq.cm on residuals

4. DESIGN OF DETECTION HYPOTHESES

Detection hypotheses are arrived at in three steps.

4.1. Formulation of D-Matrix

For these set of residual generators and faults the Detection matrix (or D-matrix) has been determined as shown in Table 2 by simulation of various faults. This matrix captures the effects of all the five faults on both measurement and parameter residuals. Here 'NF' denotes No-Fault.

Table 2. D-matrix for Estimators 1, 2 and 3

FC	Rx1	Rp1	K1	B1	Rx2	Rp2	K2	B2	Rx3	K3
F1	1	0	1	0	1	1	1	0	1	1
F2	1	1	1	0	1	1	1	0	1	1
F3	0	0	0	0	1	1	1	1	0	0
F4	1	1	1	0	1	1	1	0	1	1
F5	0	0	0	1	0	0	0	1	0	0
NF	0	0	0	0	0	0	0	0	0	0

4.2. Derivation of Fault Isolation Logic

Fault isolation logics are derived from D-matrix which are tabulated in Table 3. These isolation logics are not unique. The residuals for a particular logic are chosen based on their sensitivity to that fault. From Table 2 it can be observed that faults F2 and F4 are not isolable since the effect on all the residuals are same for both the faults. It is to be noted here that all three estimators are assumed to be running simultaneously. Since the measurement residuals contain noise there is always a chance of false alarm particularly for small decision thresholds designed to detect small faults. For parameter residuals simple threshold checking helps in detection. Increase in threshold reduce P_{FA} as well as P_D. Thus, choice of thresholds is of great importance. To determine a good threshold which will have low P_{FA} and high P_D, several ROC plots need to be considered for different fault magnitudes as described in the next section.

Table 3. Isolation logic for various faults

FC	Logic
F1	$Rx3 \cdot \overline{Rp1} \cdot \overline{B1}$
F2 or F4	$Rx3 \cdot Rp1$
F3	$\overline{Rx1} \cdot Rx2 \cdot Rp2$
F5	$B1$
NF	Otherwise

4.3. Hypotheses Design

Based on the selected fault isolation logic the corresponding detection hypothesis expression to be tested against its threshold is to be designed for each fault. The selection can be made based on the ROC plots obtained for the various detection hypotheses. From Table 3 it can be seen that for isolating F1 one may choose the complex detection hypothesis $(|Rx3| > Tx3) \cdot (|Rp1| < Tp1) \cdot (|B1| < TB1)$. It is now required to choose thresholds *Tx3*, *Tp1* and *TB1* for good P_D-P_{FA} performance for small faults. Here we consider that for acceptable performance $P_D > 0.9$ and $P_{FA} < 0.1$. Now from the D-matrix in Table 2 it is observed that for an LVDT bias fault (F1) either of *Rx1*, *Rx2* or *Rx3* may be included in the isolation logic. However, among these, one

must choose the residual which shows the maximum sensitivity to the fault F1. This can be determined from the ROCs of single residuals. It has been observed that *Rx1* and *Rx2* are equally sensitive to fault F1. From the of ROC plots of *Rx1* and *Rx3* as shown in Figures 5 and 6 it can be concluded that *Rx3* is more sensitive to F1 than *Rx1*. The numbers along the lines inside the plot are the values of thresholds for a particular fault magnitude.

Upon selection of the residual variables of the isolation logic one has to make a choice of the expression for detection hypothesis. It turns out that, due to presence of noise, checking for crossing of thresholds at single time instants is not adequate for lowering the false alarm rate significantly. Accordingly, multiple consecutive threshold crossings may have to be incorporated. Similarly certain features of the residual signal (the mean over a certain time period) may be compared with thresholds. The Detection Hypothesis (DH) chosen for F1 (Eq. 3) is:

$$DH1: \left(Rx3(k) > Tx3 \bullet Rx3(k+1) > Tx3\right) \bullet \left(\left|Mean\ (Rp1,30)\right| < Tp1\right) \bullet \left(\left|B1\right| < 200\right) \quad (3)$$

where $Mean(x,n)[k] \overset{\Delta}{=} \frac{1}{n} \sum_{j=k-n+1}^{k} x[j]$

For any fault F_i (i=1, 2 … 5) from set F = {F1, F2, F3, F4, F5, NF), the False Alarm Set (FAS) is F – {F_i}. The various values of P_D and P_{FA} for different thresholds of *Rx3* and *Rp1* for fault F1 of magnitude +0.07V and +0.09V are tabulated in Table 4 and 5, respectively.

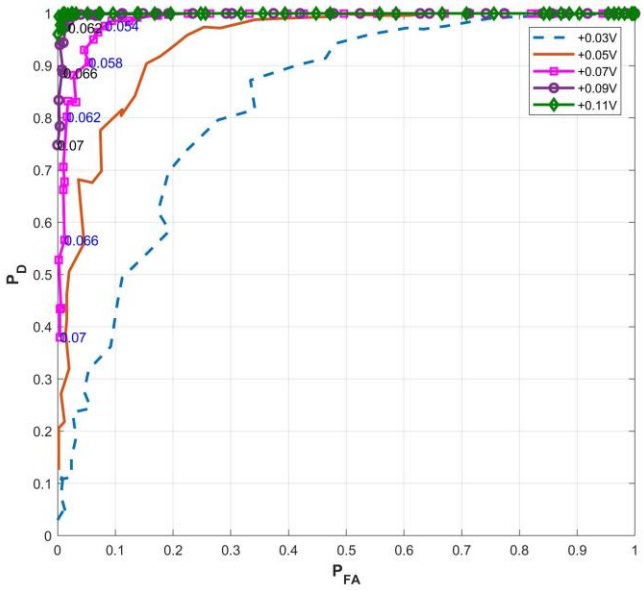

Figure 5. ROC of Rx3 at various F1 magnitudes

Figures 7 and 8 show the combined ROC plot after implementing the detection logic for fault F1 of magnitude +0.07V and +0.09V, respectively with NF being the only element in FAS.

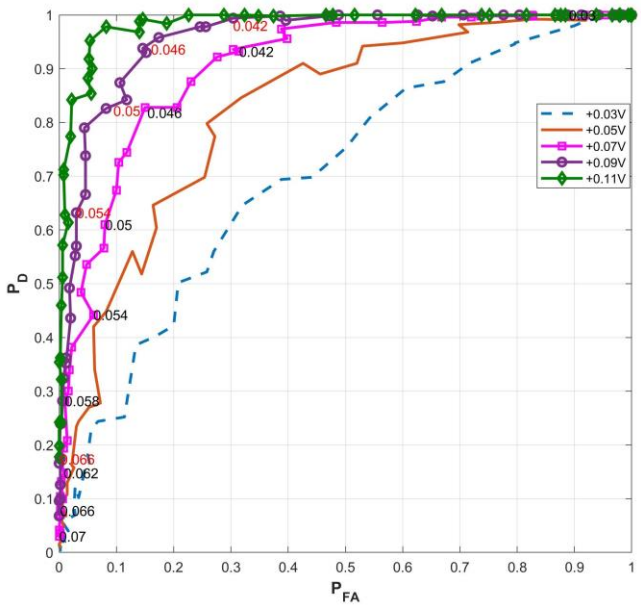

Figure 6. ROC of *Rx1* at various F1 magnitudes

Table 4. (P_D, P_{FA}) values for F1 = +0.07V

	Thresholds for *Rp1*				
Thresholds for *Rx3*	**2.4**	**2.1**	**1.8**	**1.5**	**1.2**
0.06	0.91, 0.08	0.898, 0.105	0.895, 0.095	0.913, 0.103	0.853, 0.098
0.055	0.975, 0.193	0.978, 0.17	0.968, 0.195	0.958, 0.173	0.928, 0.148

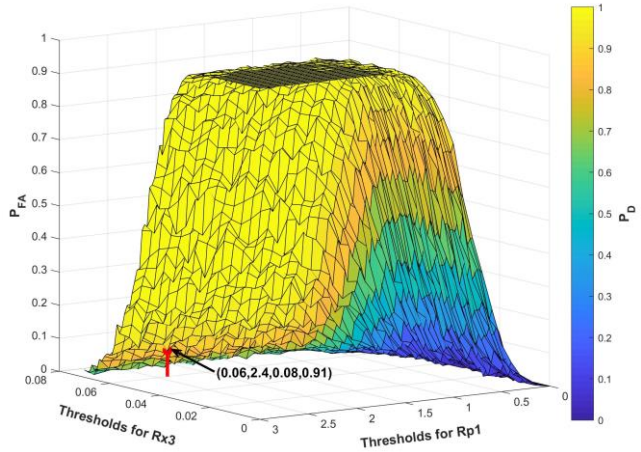

Figure 7. Joint ROC plot for F1 = +0.07V

The thresholds which result in acceptable detection performance are colored and bordered in Tables 4 and 5, respectively and the same are marked in their respective figures in the following format: (‘Threshold for *Rx3*’, ‘Threshold for *Rp1*’, ‘P_{FA}’, ‘P_D’). Figure 9 shows the

combined ROC plot after implementing the detection logic for fault F1 of magnitude +0.09V with F2 = +5 kgf/sq.cm being the only element in FAS. Table 6 contains the corresponding P_D-P_{FA} values for this plot which shows a bit poorer performance compared to that of Table 5.

Table 5. (P_D, P_{FA}) values for F1 = +0.09V

Thresholds for *Rx3* \ Thresholds for *Rp1*	3.0	2.7	2.1	1.8	1.5
0.065	0.94, 0.03	0.925, 0.018	0.955, 0.033	0.955, 0.045	0.95, 0.043
0.06	0.99, 0.093	0.983, 0.09	0.975, 0.098	0.988, 0.06	0.988, 0.123

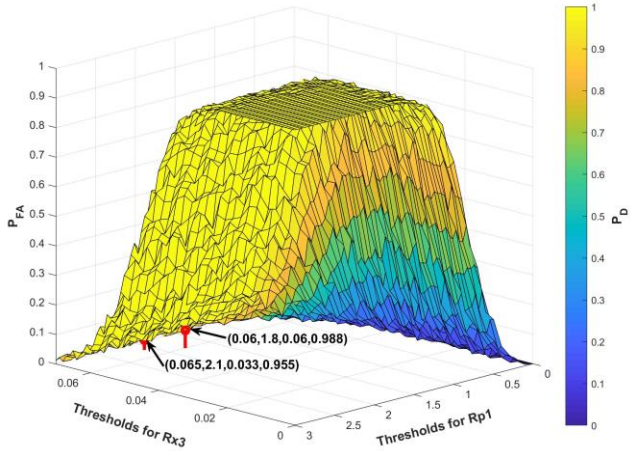

Figure 8. Joint ROC plot for F1 = +0.09V

From this observation it can be inferred that *Rx3* is highly affected by fault F2 since P_{FA} is constantly high for the shown threshold range. Looking at the D-matrix it is seen that fault F2 has same effect on the residuals as fault F1 except for *Rp1* and *Rp2*. So in the DH1 more emphasis should be given to the *Rp1* residual test statistic than *Rx3*. A suggestion can be to take mean of more than 30 samples of *Rp1* to improve the detection performance.

The characteristics of the various residuals for faults F2 and F4 are shown in Figures 10 and 11. It has been observed that for negative bias in fault F2 the Seal stiffness (K_{SD}) estimate decreases from its nominal value (which means *K3* residual deviates from zero in the positive direction). But from prior domain knowledge one can say that seal stiffness can only increase and never decrease with time. Using such knowledge it may be possible to isolate fault F4 and F2, when the *K3* residual goes positive. From the joint ROC plots of Figure 12 and 13 it can be inferred that the residuals *Rx3* and *Rp1* are highly sensitive to both faults F2 and F4, and so small changes can easily be detected. For both the plots NF is the only element in FAS.

Table 6. (P_D, P_{FA}) values for F1= +0.09V with F2= +5 kgf/sq.cm in FAS

Thresholds for *Rx3* \ Thresholds for *Rp2*	1.1	1.0
0.065	0.843, 0.095	0.803, 0.038
0.06	0.88, 0.093	0.843, 0.045
0.055	0.915, 0.075	0.855, 0.055
0.05	0.91, 0.09	0.845, 0.063
0.025	0.923, 0.088	0.855, 0.035
0.01	0.933, 0`.093	0.86, 0.058

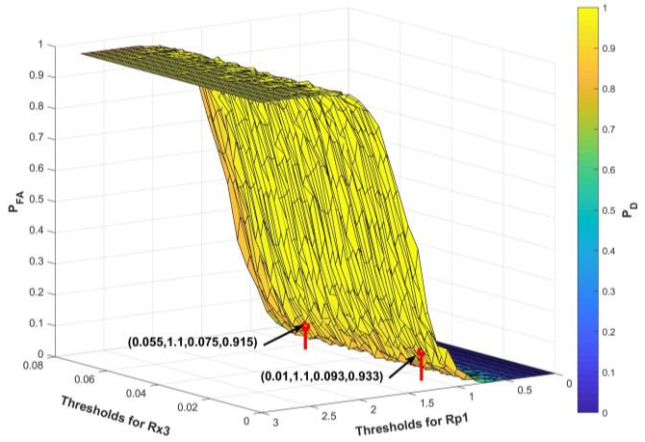

Figure 9. Joint ROC plot for F1 = +0.09V with F2= +5 kgf/sq.cm from FAS

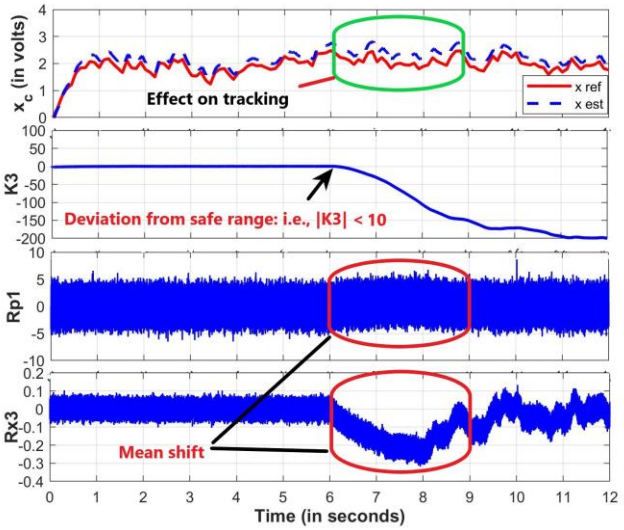

Figure 10. Effect of F2 = +5 kgf/sq.cm on residuals

The detection hypothesis to detect (F2 or F4) (Eq. 4) is given as:

$$DH2:\left(Rx3(k)>Tx3\bullet Rx3(k+1)>Tx3\right)\bullet \left(Rp1(k)>Tp1\bullet Rp1(k+1)>Tp1\right) \quad (4)$$

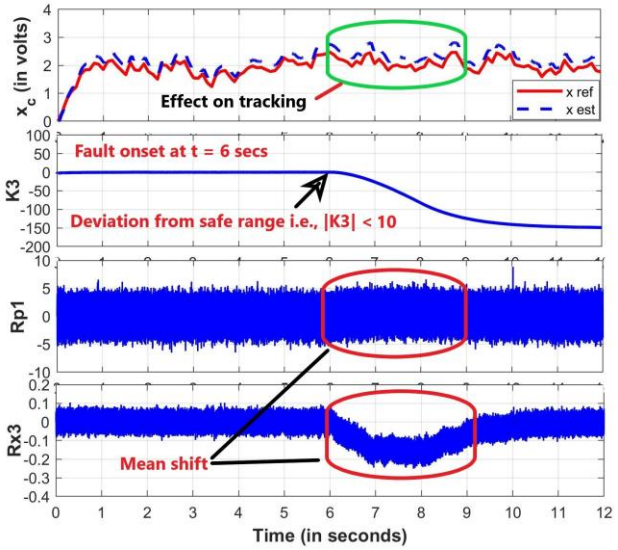

Figure 11. Effect of F4 = +150 kgm/deg on residuals

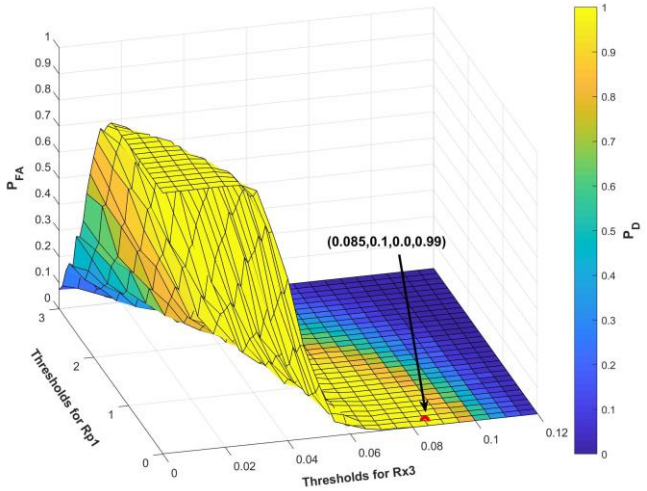

Figure 12. Joint ROC plot for F2 = +2 kgf/sq.cm

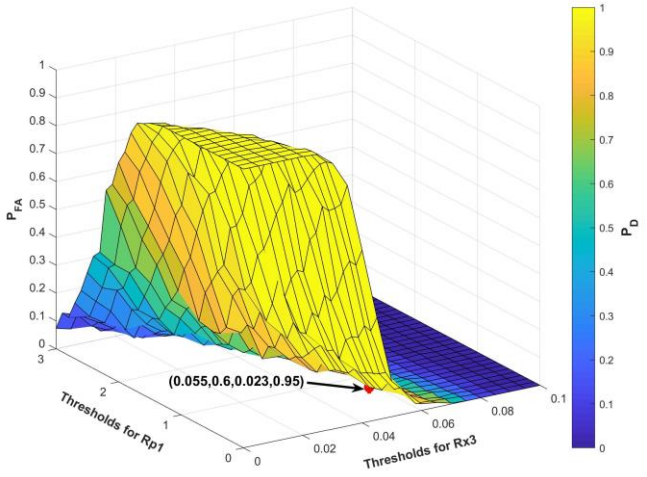

Figure 13. Joint ROC plot for F4 = +60 kgm/deg

5. CONCLUSION

In this work a systematic procedure to obtain improved FDI performance has been developed and illustrated based on numerical simulation of a detailed nonlinear dynamic model of an EHA. It is demonstrated that, using multiple residuals from several estimators, one can formulate complex detection hypotheses and tune their thresholds based on ROC plots to yield superior P_D-P_{FA} performance. Experimental validation of the conclusions of the numerical study and theoretical analysis and optimization of performance remain the two major directions for future research.

ACKNOWLEDGEMENT

It is gratefully acknowledged that this research is partially supported by the project HEV of SRIC IIT Kharagpur which is jointly funded by TATA Motors and Govt. of India under UAY scheme.

NOMENCLATURE

x	Position of the actuator in cm which is measured using LVDT as $K_{pfb} \times x$ (in $volts$)
v	Velocity of the actuator in cm/s
a	Actuator area in cm^2
K_{SD}	Seal stiffness in $kgm/\deg$
m	Equivalent load mass in kg
l_T	Torque arm length in cm
b_{eq}	Friction coefficient in $kg/cm/s$
P_m	Differential pressure in kgf/cm^2
Q_d	Flow rate in cc/s
ω_v	Servo bandwidth in rad/s
Co	Control valve spool gain in $cm^4/\sqrt{kg}/s/mA$
K_v	Servo valve gain in mA/V
K_p	Proportional gain of controller
K_i	Integral gain of controller in s^{-1}
K_{pfb}	Feedback gain in $volts/cm$
x_c	Reference position of the actuator in cm
β	Bulk modulus of hydraulic fluid in kg/cm^2
V_o	Entrapped volume in cc
C_{2g}	Flow pressure coefficient in $cc/s/kg/cm^2$
ks	Servo valve gain
r	Radius of armature from center to pole face mm

REFERENCES

An, L., & Sepehri, N. (2003). Hydraulic actuator circuit fault detection using extended kalman filter.

Proceedings of the 2003 American Control Conference (vol. 5, pp. 4261-4266), June 4-6, Denver, CO. doi: 10.1109/ACC.2003.1240505

An, L., & Sepehri, N. (2005). Hydraulic actuator leakage fault detection using extended Kalman filter. *International Journal of Fluid Power*, vol. 6(1), pp. 41-51. doi: https://doi.org/10.1080/14399776.2005.10781210

Blanke, M., Kinnaert, M., Lunze, J., Staroswiecki, M., & Schröder, J. (2006). *Diagnosis and fault-tolerant control* (Vol. 2). Berlin: springer.

Chinniah, Y., Burton, R., & Habibi, S. (2003). Viscous Damping Coefficient and Effective Bulk Modulus Estimation in a High Performance Hydrostatic Actuation System using Extended Kalman Filter. *International Journal of Fluid Power*, vol. 4(3), pp. 27-34. doi: 10.1080/14399776.2003.10781172

Chinniah, Y., (2004). *Fault detection in the electrohydraulic actuator using extended Kalman filter*. Doctoral dissertation. University of Saskatchewan, Saskatoon, Canada

Ding, S. X. (2008). Model-based fault diagnosis techniques: design schemes, algorithms, and tools. London: Springer Science & Business Media

Frank, P. M. (1990). Fault diagnosis in dynamic systems using analytical and knowledge-based redundancy: A survey and some new results. *Automatica*, vol. 26(3), pp. 459-474. doi: https://doi.org/10.1016/0005-1098(90)90018-D

Halder, P., Mukhopadhyay, S., Chaudhuri, S. K., & Ghoshal, T. K. (2012). Detection and Diagnosis of Process and Sensor Faults in Electro-hydraulic Actuator using Extended Kalman Filter (EKF). *Proceedings of Advances in Control and Optimization of Dynamic Systems*

Hajian-Tilaki, K. (2013). Receiver operating characteristic (ROC) curve analysis for medical diagnostic test evaluation. *Caspian journal of internal medicine*, vol. 4(2), pp. 627-635

Isermann, R. (2006). *Fault-diagnosis systems: an introduction from fault detection to fault tolerance*. Berlin: Springer Science & Business Media

Kay, S. M. (1998). *Fundamentals of statistical signal processing, Volume II: Detection theory*. Upper Saddle River, NJ, USA: Prentice Hall PTR

Kumar, R., & Indrayan, A. (2011). Receiver operating characteristic (ROC) curve for medical researchers. *Indian pediatrics*, vol. 48(4), pp. 277-287.

Merritt, H. (1967). *Hydraulic control systems*. New York: John Wiley & Sons

Metz, C. E. (2006). Receiver operating characteristic analysis: a tool for the quantitative evaluation of observer performance and imaging systems. *Journal of the American College of Radiology*, vol. 3(6), pp. 413-422

Trachi, Y., Elbouchikhi, E., Choqueuse, V., Benbouzid, M. E. H., & Wang, T. (2017). A novel induction machine fault detector based on hypothesis testing. *IEEE Transactions on Industry Applications*, vol. 53(3), pp. 3039-3048. doi: 10.1109/TIA.2016.2625769

Wan, E. A., & Nelson, A. T. (2001). Dual extended Kalman filter methods. *Kalman filtering and neural networks*, pp.123-174, New York: Wiley

BIOGRAPHIES

Desham Mitra received his B.Tech in Electrical Engineering from NIT Agartala, India in 2013 and M. Tech in Electrical Engineering with Control System as specialization from IIEST Shibpur, India in 2016. He is currently working towards his PhD degree in Electrical Engineering from IIT Kharagpur, India. His research areas include development of Lithium ion battery management systems for hybrid and electric vehicles and fault diagnosis of complex engineering systems.

Pulak Halder received his B.E. and M.E. from the Department of Electrical Engineering, Jadavpur University, India in 1995 and 1998, respectively. He is working as Scientist at RCI, DRDO, India, at present. His research interests include fault detection and isolation and hardware-in-loop simulation.

S. Mukhopadhyay received his B.Tech. (Hons.), M.Tech. and PhD., all from IIT Kharagpur in 1985, 1987,and 1991, respectively. He is a Professor in the Department of Electrical Engineering, IIT Kharagpur, at present. His current research interests are in automotive control, fault diagnosis and prognosis, battery management systems and industrial automation.